VIII International Conference on Particle-Based Methods
PARTICLES 2023
U. Perego, M. Cremonesi, A. Franci (Eds)

CONTACT DETECTION ALGORITHM FOR CONVEX NURBS PARTICLES

M. V. CRAVEIRO[1], A. GAY NETO[1] AND P. WRIGGERS[2]

[1] Department of Structural and Geotechnical Engineering, Polytechnic School
University of São Paulo
São Paulo, Brazil
e-mail: marina.craveiro@usp.br, alfredo.gay@usp.br, https://ppgec.poli.usp.br/en/

[2] Institute of Continuum Mechanics, Faculty of Mechanical Engineering
Leibniz Universität Hannover
Hannover, Germany
email: wriggers@ikm.uni-hannover.de, https://www.ikm.uni-hannover.de/en/our-institute

Abstract. The present work proposes a contact detection algorithm for convex particles whose boundaries are mathematically defined by non-uniform B-splines (NURBS). This algorithm involves a hierarchy of contact searches, including both global and local steps. The focus is on the formulation of the local contact problem (LCP) using a master-to-master approach. It is based on computer graphics and optimization techniques. Besides the algorithm, the paper also discusses strategies for modeling particle geometry and their implications in contact detection. The use of multiple parameterizations (patches) assembled in space, for instance, provides more flexibility in the construction of particles and avoids numerical singularities. However, it leads to local geometric imperfections at the connection between patches. The LCP formulation proposed herein can deal with such imperfections through a contact degeneration technique. An example shows the robustness of the method.

Keywords: Computer Graphics, Contact, Degeneration, Discrete Element Method, NURBS.

1 INTRODUCTION

In numerical simulations using the discrete element method (DEM) [1], particle geometry influences the system behavior in two ways. First, the rotational motion of particles depends on their mass distribution, which is related to particle geometry. Second, geometry also governs the interaction between particles, which predominantly results from contact in mechanical systems. The contact contribution to the system is given by normal and tangential forces applied to particles, whose location and direction are related to the contact interface geometry.

Real particle geometries can be simplified, for instance, by spheres [1], ellipsoids [2], polyhedral [3], cluster/clump of spheres [4], level set functions [5] and non-uniform rational B-splines (NURBS)[6,7]. A compatible contact model must be used for each geometry [8–10].

To reduce computational cost, the contact detection in DEM simulations is usually performed by hierarchical steps, from less accurate levels (global steps) to more accurate ones (local steps). The idea is to first eliminate improbable pairs of contact. Only those pairs of elements that have a real chance of establishment of contact will be subjected to a more rigorous contact investigation, in which real geometry is fundamental.

For convex particles whose boundaries are defined by NURBS surfaces, [7] introduces a formulation for the local contact problem (LCP) using a master-to-master approach, where the contact is pointwise, no contact points are chosen *a priori*, and penetrations are allowed and related to local deformations. The LCP formulation is based on computer graphics and optimization techniques [9], which enable us to determine the contact status (active or not), besides determining the maximum penetration through minimization problems.

The content of the present paper is an improvement of the previous contact formulation [7] that allows us to deal with simulations with a more reasonable number of particles. Aiming at developing a complete contact detection algorithm for convex NURBS particles, the paper describes how to incorporate the previous formulation into the automatic contact detection framework developed by [11], which involves both global and local contact searches. The paper also discusses strategies for modeling the geometry of NURBS particles and how they can influence the numerical solution of the LCP. When using multiple parameterizations, for example, the connection between them is a source of geometric imperfections, where the behavior of the LCP solution is not predictable. To overcome numerical issues, a contact degeneration technique based on [12] is proposed, which consists in the main contribution of the research for enabling the use of more general geometries in DEM simulations. The simulations are performed in the software *Giraffe* [13]. The software *Rhinoceros 3D* [14] helps with the construction of NURBS surfaces.

2 NURBS AND MODELING OF PARTICLES

The boundary of a particle can be represented by parameterized surfaces with general form

$$\Gamma(\zeta,\theta) = \boldsymbol{x}_0 + \boldsymbol{Q}_0\boldsymbol{s}(\zeta,\theta), \tag{1}$$

in which $\mathbf{x}_0$ and $\mathbf{Q}_0$ represent a translation vector and a rotation tensor, respectively, both relative to a global coordinate system. $\mathbf{s}(\zeta,\theta)$ is the surface parameterization relative to a local coordinate system.

NURBS surfaces defined by [15]

$$\boldsymbol{s}(u,v) = \frac{\sum_{i=0}^{n}\sum_{j=0}^{m} N_{i,p}(u)N_{j,q}(v)w_{i,j}\boldsymbol{p}_{i,j}}{\sum_{i=0}^{n}\sum_{j=0}^{m} N_{i,p}(u)N_{j,q}(v)w_{i,j}} \tag{2}$$

can be chosen to parameterize particle boundaries. It maps a rectangular parametric space defined by orthogonal directions u and v into a surface region $\mathbf{s}(u,v)$ in geometric space, herein named as NURBS patch. $N_{i,p}(u)$ and $N_{j,q}(v)$ are piecewise polynomial basis functions with degrees p and q, $\mathbf{p}_{i,j}$ are control points, $w_{i,j}$ are weights, $n+1$ and $m+1$ are the number of control points associated with u and v, respectively. The parameters u and v, common in NURBS literature, are equivalent to parameters ζ and θ defined for the contact formulation.

Two different strategies can be employed to model the boundary of particles using NURBS surfaces, see Figure 1. In the first, only one patch is used to generate the entire particle. Note that the particle boundary is a closed surface, and the parametric space and real surface topologies do not match. Consequently, using one parameterization generates singularities that do not exist in real geometries: poles and seam, as illustrated in Figure 1a. Poles are material points associated with different pairs of parameters u and v. Derivatives with respect to one of these parameters are zero at poles, which is not welcome in numerical procedures. The seam, in its turn, defines at the same curve the beginning and the end of the parametric space in direction u or v. So, it is necessary to predict the change of parameters close to this curve.

Another strategy to model the boundary of particles is to use multiple patches properly assembled in space, especially rectangular patches whose topology is matchable to NURBS parametric space. See Figure 1b. For more complex geometries, this second strategy provides flexibility in modeling, also eliminating poles. However, it is still necessary to manage the change of parameters at the connection between different parameterizations. Besides this, the connection between patches becomes a source of geometric imperfections, since it is difficult to ensure connections at which convexity and smoothness are maintained. These are mandatory conditions for the adequate behavior of the LCP solution proposed in [7].

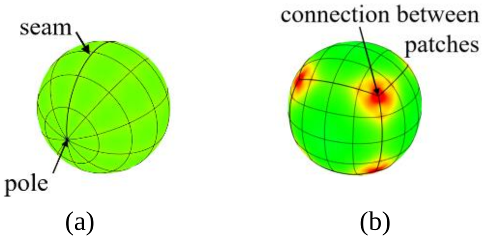

Figure 1: Modeling NURBS particles with (a) one patch (b) multiple patches (different colors are related to different curvatures)

Each modeling strategy has its own issues to be handled. In the present work, particles are modeled with multiple patches. Six patches are used, which gives flexibility in modeling and guarantees rectangular topology of patches. For contact detection purposes, the geometric imperfections can be overcome with the contact degeneration technique described in Section 3.

3 CONTACT DETECTION ALGORITHM

In DEM simulations, for each time step of the time integration and for each pair of particles, it is necessary to verify if contact takes places and, if so, to quantify the maximum penetration that will be used to evaluate contact forces. This section briefly presents a contact detection algorithm for particles modeled with multiple NURBS patches. A complete description of such algorithm can be found in [7,11,16].

Only convex particles are considered herein. Thus, only a single pointwise contact can occur for each pair of particles. The search for such single contact is hierarchically divided into three steps. The first two steps are related to coarser searches for contact while the last one deals with contact at a more precise local level.

3.1 Global contact search

If no constraints are imposed, in principle, all particles of the system can establish contact with each other. However, locally analyzing the contact between all possible combinations of particles is not feasible. The computational cost would be extremely high. Thus, in practice, it is assumed that the contact between two particles only occurs if they are close enough to each other. To verify such proximity and to eliminate improbable pairs of contact, one may employ bounding volumes wrapping the original geometries. If a pair of bounding volumes is not overlapping, the related pair of geometries is also not candidate to contact. In general, contact tests between bounding volumes are well-known and low-cost [17].

Assuming that NURBS particles are modeled with six patches, the present contact algorithm works with two levels of global search. For the first level, spheres wrapping the entire NURBS particles are constructed. The center of such spheres coincides with particle centroid. Considering only positive weights $w_{i,j}$ for NURBS, it is guaranteed that the control points are external to the particles. Thus, the radius of the spheres can be assumed as the distance from their center to the furthest NURBS control point $\mathbf{p}_{i,j}$. To check if two bounding spheres A and B are overlapping, one may evaluate

$$\delta = r_A + r_B - dist_G, \tag{3}$$

which is positive in case of contact. r_A and r_B are the radii of spheres A and B, respectively, and $dist_G$ represents the distance between their centroids.

For those particles whose bounding spheres are overlapping, a second level of global contact search is performed. The idea is to construct bounding volumes wrapping each of the six NURBS patches. Initially axis-aligned bounding boxes are constructed from the furthest control points along each global direction x, y and z. Although these boxes are initially aligned with the global coordinate system, they move together with particles, experiencing the same displacements and rotations. So, to verify if the bounding boxes are overlapping, it is necessary to employ algorithms that can be applied to any box orientations. One may use either the GJK algorithm or the separating-axis test [17].

The global contact search results in a list of pairs of patches candidate to contact. Determining such pairs of patches directs the LCP to the regions of the particles at which the contact can occur. Only one pointwise contact is to be found per pair of convex particles.

3.2 Local contact search

3.2.1 General formulation

The interaction between particles A and B is represented by normal and tangential contact forces applied to such particles. These forces are evaluated by using the gap vector

$$\boldsymbol{g} = \Gamma_A(\zeta_A, \theta_A) - \Gamma_B(\zeta_B, \theta_B) \tag{4}$$

evaluated at contact points, where $\mathbf{g}$ is parallel to the external normals of Γ_A and Γ_B.

As we allow small penetrations between particles, when there is contact, $\mathbf{g}$ corresponds to the maximum penetration at the LCP solution. Otherwise, $\mathbf{g}$ represents the distance between particles. Thus, for those pairs of patches resulting from the global contact detection, the LCP verifies more accurately if contact occurs. If so, it determines the maximum penetration.

To start, one can define the objective function

$$f_1 = \frac{1}{2}||\boldsymbol{g}||^2 = \frac{1}{2}||\Gamma_A(\zeta_A, \theta_A) - \Gamma_B(\zeta_B, \theta_B)||^2, \tag{5}$$

which gives distances between patches. To check the occurrence of contact, one has to minimize f_1 with variables ζ_A, θ_A, ζ_B and θ_B. If the minimum is positive, Γ_A and Γ_B are spaced apart with distance $\|\mathbf{g}\|$. Otherwise, there is contact between them, and the minimum is related to an intersection point. The maximum penetration is a saddle point of f_1 [9].

After detecting contact with f_1, one can define another objective function

$$f_2 = \frac{1}{2}\|\boldsymbol{g}\|^2 = \frac{1}{2}\left\|\Gamma_A\big(\zeta_A(\rho,\varphi),\theta_A(\rho,\varphi)\big) - \Gamma_B\big(\zeta_B(\rho,\varphi),\theta_B(\rho,\varphi)\big)\right\|^2, \tag{6}$$

whose minimization leads to the maximum penetration between Γ_A and Γ_B. In Eq. (6), the surface parameters $\zeta_A, \theta_A, \zeta_B$ and θ_B are dependent on the azimuth and elevation angles ρ and φ, respectively, which define directions $\mathbf{d}$ in space.

The relationship between surface parameters and angles in space comes from computer graphics concepts. Defining the configuration space obstacle (CSO) as the set of points $\Gamma_A(\zeta_A,\theta_A) - \Gamma_B(\zeta_B,\theta_B)$, it is known that the maximum penetration is the minimum distance between points $\mathbf{map}_{CSO}$ on the CSO boundary and its origin [7]. Distances $\mathbf{map}_{CSO}$ on the CSO boundary can be obtained with the support mapping

$$\boldsymbol{map}_{CSO}(\boldsymbol{d}) = \boldsymbol{map}_{\Gamma_A}(\boldsymbol{d}) - \boldsymbol{map}_{\Gamma_B}(-\boldsymbol{d}), \tag{7}$$

where

$$\boldsymbol{d}\cdot\boldsymbol{map}_{\Gamma}(\boldsymbol{d}) = max\,\{\boldsymbol{d}\cdot\boldsymbol{x}_{\Gamma} \mid \boldsymbol{x}_{\Gamma} \in \Gamma\}. \tag{8}$$

Observe that the minimization of f_2 searches for angles ρ and φ that define a direction $\mathbf{d}$ related to the maximum penetration between Γ_A and Γ_B. Such minimization can be performed by the trust-region Newton method [18]. Each iteration of the minimization of f_2 is related to a direction $\mathbf{d}$. The corresponding parameters ζ_A, θ_A, ζ_B and θ_B are then obtained by applying the support mapping given in Eq. (8) to surfaces Γ_A and Γ_B with $\mathbf{d}$. Eq. (8) can be understood as optimization problems with objective functions

$$f_{sup\Gamma} = \pm\boldsymbol{d}\cdot\,\boldsymbol{map}_{\Gamma}(\boldsymbol{d}) = \pm\boldsymbol{d}\cdot\,\Gamma(\zeta,\theta). \tag{9}$$

Regardless the optimization method, it is necessary to evaluate the gradient ∇f_2 and the Hessian $\nabla^2 f_2$ for each iteration. The objective function f_2 is a composite function, i.e., it depends on parameters ζ_A, θ_A, ζ_B and θ_B that, in their turn, depend on angles ρ and φ. So, the elements of ∇f_2 and $\nabla^2 f_2$ depend on the derivatives of the surfaces with respect to their parameters as well as on the derivatives of such parameters with respect to the angles ρ and φ. The former can be obtained using the procedures given in [15], and the latter can be obtained by implicitly differentiating Eq. (9) with respect to angles ρ and φ, which results on linear systems of equations in the traditional form $\mathbf{Ax} = \mathbf{b}$. For more details on how to minimize f_2, see [7].

3.2.2 Contact detection at connection between NURBS patches

Solving the LCP for regions close to the connection between patches implies in dealing with different surface parameterizations. The solution can leave the valid range of parameters of the current patch. Thus, the formulation has to be able to detect to which patch the solution has to migrate and to change parameterizations. This can be done by storing the connectivity between patches. Rectangular patches are assumed herein and, therefore, each one has four neighboring patches, which do not change throughout the simulation. See Figure 2.

Whenever a parameter ζ or θ leaves its valid range $[\zeta_i,\zeta_f]$ or $[\theta_i,\theta_f]$ during the solution of the LCP, the closest limit value is imposed. Using connectivity information, the change of patch is performed projecting the point of the current patch, related to the limit value ζ_i, ζ_f, θ_i or θ_f, onto its neighboring patch. If both parameters ζ and θ are out of range, the neighboring patch is not known *a priori*. It can be related either to directions ζ or θ. So, we assume herein that the neighboring patch in direction ζ is firstly chosen. If the next solution continues out of range, the neighboring patch in direction θ is chosen alternatively.

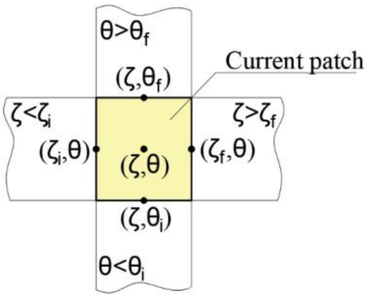

Figure 2: Connectivity between patches

If the solution permanently migrates to neighboring patches different from the initial ones, we assume that the latter are not prone to contact each other. All particles are convex, and the solution is unique and related to only one pair of patches. Thus, the solution will be found and accepted when working with the LCP related to the patches to which the solution migrates.

3.2.3 Degeneration technique

As described in Section 2, the connection between patches is not free of local geometric imperfections. Even if all NURBS attributes are intentionally adjusted to generate smooth and convex connections, there are numerical imprecisions that locally eliminate such conditions. With that, the change of patches described in Section 3.2.2, which is theoretically well-behaved, becomes unpredictable and causes undesirable stops in the numerical simulation. These situations consist in local issues that should not compromise the overall response of the system. Thus, whenever the LCP does not converge at the connection between patches, it uses the degeneration technique, which is adapted from [12] and is described below.

The LCP formulation searches for parameters $\zeta_A, \theta_A, \zeta_B$ and θ_B that correspond to points candidate to contact on surfaces Γ_A and Γ_B, respectively. Even when minimizing Eq. (6), whose variables are the angles ρ and φ, the corresponding parameters are found by using support mappings. The degeneration technique [12] imposes fixed values to one or more of such parameters according to the connection region. Thus, it reduces the number of parameters to be found.

When convergence is not achieved by the LCP in regions between two neighboring patches, the parameter related to the direction of connection is fixed. The search for the contact point is then restricted to the curve that separates the patches, i.e., instead of two parameters, there is only one to be found. For regions near the connection between three patches, one may fix both parameters at the node shared by the three patches, i.e., the two parameters are known *a priori*.

Let

$$\boldsymbol{c} = [\zeta_A \quad \theta_A \quad \zeta_B \quad \theta_B]^T \tag{10}$$

be the surface parameters written in the vector form. The degeneration level is the number of parameters that are not variables of the LCP, i.e., whose values are fixed [12]. The number of remaining parameters is called s. They are free and can be grouped into a vector $\mathbf{c}_{\mathrm{s}}$ with dimension s. The contact degeneration transforms $\mathbf{c}$ to $\mathbf{c}_{\mathrm{s}}$ with the aid of a degenerative operator $\mathbf{P}_{\mathrm{s}}$ in such a way that

$$\boldsymbol{c}_s = \boldsymbol{P}_s^T \boldsymbol{c}. \tag{11}$$

If s is equal to four, $\zeta_{\mathrm{A}}, \theta_{\mathrm{A}}, \zeta_{\mathrm{B}}$ and θ_{B} have to be found. There is no degeneration. On the other hand, if s is equal to zero, $\zeta_{\mathrm{A}}, \theta_{\mathrm{A}}, \zeta_{\mathrm{B}}$ and θ_{B} are imposed.

Reducing the number of parameters to be found, the number of equations of the optimization processes also reduce. For each iteration of the minimization of f_2, Eq. (9) has also to be minimized to find the surface parameters related to angles ρ and φ. Eq. (9) represents systems of two equations related to parameters of each patch. Two situations can occur when contact degeneration is called. Either ζ or θ is fixed or both of them are fixed for each patch. In the former, the number of equations of a patch in Eq. (9) reduces from two to one. In the latter, the system of equations does not need to be solved. The solution is readily known.

The solution of Eq. (9) can be generalized by employing degenerative operators $\mathbf{P}_{\mathrm{s}\Gamma}$ in the gradient and the Hessian of $\mathrm{f}_{\mathrm{sup}\Gamma}$, as follows

$$\nabla f_{sup\Gamma\_s} = \boldsymbol{P}_{s\Gamma}^T \nabla f_{sup\Gamma}, \tag{12}$$

$$\nabla^2 f_{sup\Gamma\_s} = \boldsymbol{P}_{s\Gamma}^T \nabla^2 f_{sup\Gamma} \boldsymbol{P}_{s\Gamma}. \tag{13}$$

$\mathbf{P}_{\mathrm{s}\Gamma}$ encompasses the parameters related to each patch, and they can be obtained by dismembering $\mathbf{P}_{\mathrm{s}}$.

After determining the set of parameters of the current iteration, the linear systems of equations used to find the derivatives of such parameters with respect to the angles ρ and φ have also to be adapted to consider contact degeneration. These systems of equations can be rewritten as

$$\boldsymbol{A}_s \boldsymbol{x} = \boldsymbol{b}_s, \tag{14}$$

where

$$\boldsymbol{A}_s = \boldsymbol{P}_{s\Gamma}^T \boldsymbol{A} \boldsymbol{P}_{s\Gamma} \text{ and } \boldsymbol{b}_s = \boldsymbol{P}_{s\Gamma}^T \boldsymbol{b}. \tag{15}$$

In summary, degeneration is a strategy employed together with the LCP formulation proposed in [7] to avoid simulations from aborting due to isolated local problems. With the degenerative operators, the LCP can be solved for both degenerated and non-degenerated cases.

4 DEM SIMULATION

The contact detection algorithm presented in Section 3 was implemented in software *Giraffe* [13], which allows us to perform DEM simulations. The output of such contact detection is the gap $\mathbf{g}$, which is used to evaluate normal and tangential contact forces. These contact forces are evaluated herein through the penalty method, as follows:

$$\boldsymbol{f}_n = \epsilon_n \boldsymbol{g} + c_n \dot{\boldsymbol{g}}_n, \tag{16}$$

$$\boldsymbol{f}_t = \epsilon_t \boldsymbol{g}_t + c_t \dot{\boldsymbol{g}}_t, \tag{17}$$

where $\mathbf{f}_\mathrm{n}$ is the normal contact force and $\mathbf{f}_\mathrm{t}$ is the trial tangential contact force. Both forces have elastic and dissipative contributions, in which ϵ_n is the normal penalty, ϵ_t is the tangential penalty, c_n is the normal damping, c_t is the tangential damping, $\dot{\mathbf{g}}_\mathrm{n}$ is the time-derivative of $\mathbf{g}$ in the normal direction and $\dot{\mathbf{g}}_\mathrm{t}$ is the time-derivative of $\mathbf{g}$ in the tangential direction. The tangential contact force follows the Coulomb's law, where $\|\mathbf{f}_\mathrm{t}\| \leq \mu\|\mathbf{f}_\mathrm{n}\|$ and μ is the coefficient of friction. Post-treatment of contact is not scope of the paper. The complete description of the penalty method implemented in *Giraffe* [13] as well as the time integration can be found in [19,20].

An example of DEM simulation will be presented below. It consists of 112 particles that are deposited and compacted inside a cubical box with a side length of 25 cm. Three sizes of particles are used. Particles A, B and C are rigid bodies with specific mass 2700 kg/m^3. Their volumes and inertia tensors are summarized in Table 1.

Table 1: Rigid body data of particles A, B and C

Element	Volume (cm^3)	Inertia tensor **J** (kg.cm^2)*
particle A	98.57	$\begin{bmatrix} 84.951 & 0.945 & -5.413 \\ 0.945 & 101.026 & 0.000873 \\ -5.413 & 0.000873 & 83.349 \end{bmatrix} . 10^{-2}$
particle B	50.47	$\begin{bmatrix} 27.837 & 0.310 & -1.774 \\ 0.310 & 33.104 & 0.000286 \\ -1.774 & 0.000286 & 27.312 \end{bmatrix} . 10^{-2}$
particle C	21.29	$\begin{bmatrix} 6.606 & 0.0735 & -0.421 \\ 0.0735 & 7.856 & 0.0000679 \\ -0.421 & 0.0000679 & 6.481 \end{bmatrix} . 10^{-2}$

* **J** is provided with respect to local barycentric axes

The boundaries of particles A, B and C are constructed with six NURBS patches. For each patch, the basis functions are cubic polynomials, the range of each parameter is [0,2], and there are 6 x 6 control points. The sides of the box are also defined by NURBS surfaces. Their basis functions are linear polynomials, and there are 2 x 2 control points.

The numerical simulation starts with the generation of a pack of particles. See Figure 3a to Figure 3d. In the first step of the simulation, a first layer is created by releasing 14 particles inside the box. We use five particles of type A (blue), three particles of type B (yellow) and six particles of type C (red). Figure 3a illustrates the initial distribution of particles inside the box, which was chosen at random. The particles are then released under the action of their self-weight in z-direction, settling at the bottom of the box after 2 s, as shown in Figure 3b.

Figure 4 shows the evolution of energy over time for the first step of the simulation. The kinetic energy is minimized to approximately zero after 2 s. The mechanical energy, in its turn, is reduced at the beginning of the simulation due to the first impacts between particles and box. After that, it remains practically constant.

In the second step of the simulation, the first layer of particles is replicated eight times over a height of 50 cm, totalizing 112 particles, as shown in Figure 3c. The particles are again released under gravity, and the final configuration shown in Figure 3d is obtained after 2.5 s.

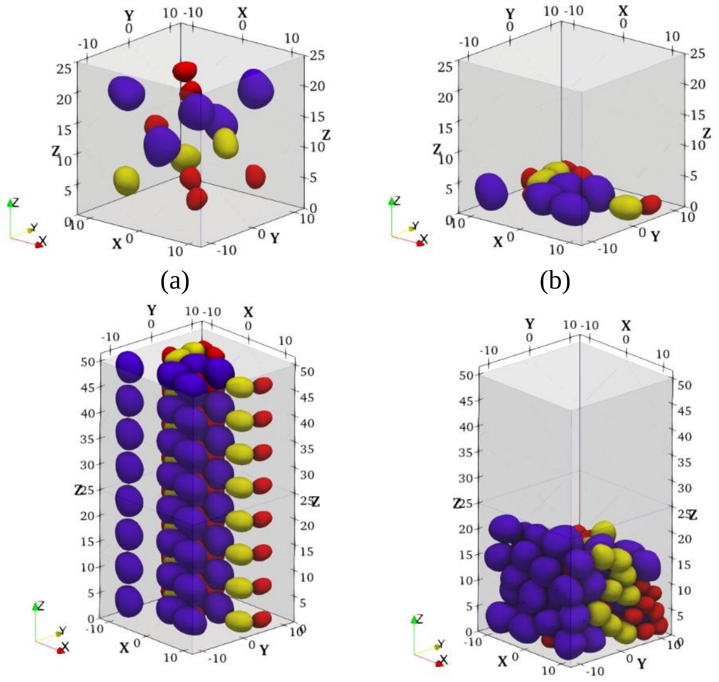

(a) (b) (c) (d)

Figure 3: Generation of a pack of particles (a) step 1: initial configuration (b) step 1: final configuration after 2 s (c) step 2: initial configuration (d) step 2: final configuration after 2.5 s, dimensions in centimeter

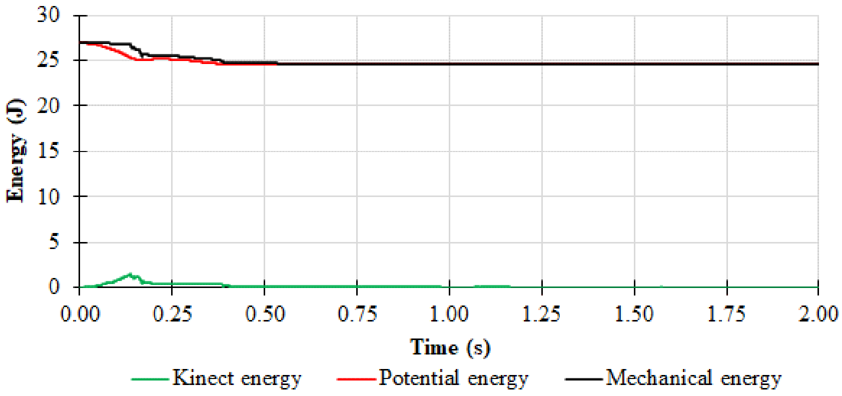

Figure 4: Step 1: energy evolution

To analyze the role of the contact degeneration in the DEM simulation, Figure 5 presents some contact outputs. It is shown the number of contacts that are monitored along the second step of the simulation, i.e., the number of LCPs to be solved for the pairs of patches that were not eliminated in the global contact search. It also shows the number of contacts that are active and how many of these active contacts employ the degeneration technique. In general, the number of degenerated contacts is not significant along the simulation. They are less than 5% of the total number of active contacts. However, without the technique described in Section 3.2.3, the numerical simulation would have been aborted due to non-convergence in the solution of the LCP at the connection between patches.

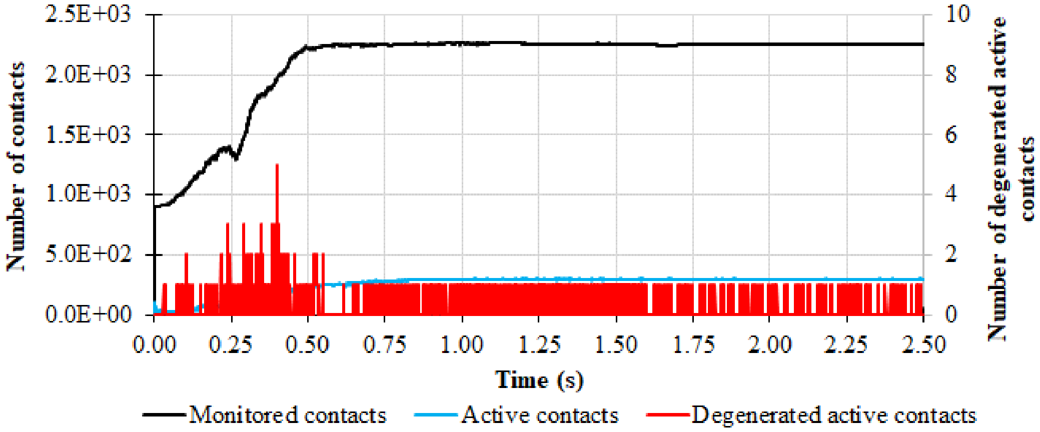

Figure 5: Step 2: contacts

The pack of particles is compacted inside the box in the third step of the simulation. For that, a lid positioned over the particles is vertically shifted eight centimeters downwards during 1 s. See Figure 6a and Figure 6b for the initial and final arrangements of particles. After compaction, the lid is lifted back to its starting position. This fourth step is depicted in Figure 6c. Figure 7 depicts the lid reaction versus displacement. Since there is dissipation of energy due to friction, it is possible to observe a small accommodation of particles.

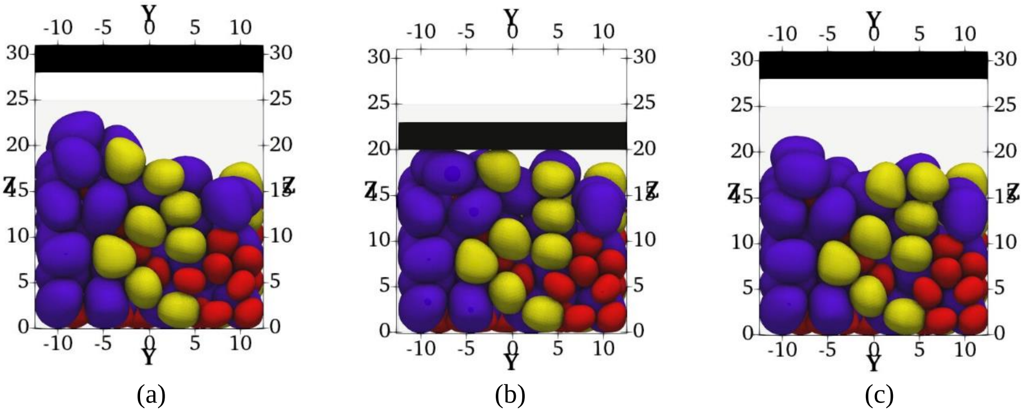

Figure 6: Compaction (a) step 3: initial configuration (b) step 3: final configuration after 1 s (c) step 4: final configuration after 1 s, dimensions in centimeter

In order to obtain small penetrations between bodies, the penalty parameters ϵ_n and ϵ_t are selected as 10^5 N/m and 10^4 N/m, respectively. The normal damping is $c_n = 10^2$ N.s/m, and the coefficient of friction is $\mu = 0.5$. The chosen initial time step is 0.001 s.

The numerical simulation indicates that the contact detection algorithm herein proposed is able to qualitatively capture the expected behavior of the system. The focus of research is exactly on this robustness of the contact algorithm. Efficiency and optimization are not scope herein. It is known, however, that they are extremely important to make the simulation feasible, being essential to study the topic in the future sequence of the research.

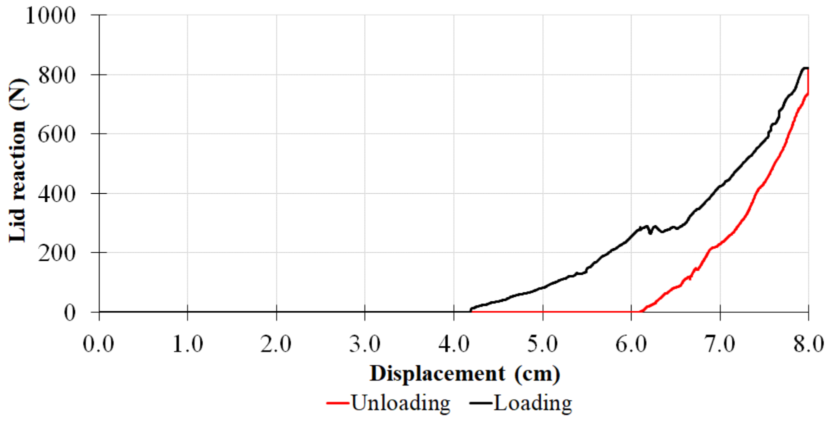

Figure 7: Steps 3 and 4: lid reaction versus displacement

5 CONCLUSIONS

The paper presented a complete contact detection algorithm for particles modeled with multiple NURBS patches assembled in space, which is based on [7,11,16]. This algorithm encompasses two levels of global contact searches as well as a local contact scheme. All levels of the contact detection rely on computer graphics techniques. The LCP also uses optimization schemes to verify contact status and to determine the maximum penetration between particles.

Besides the contact detection algorithm itself, the paper also discusses strategies to model the boundary of particles using NURBS surfaces. Implications of such strategies in the LCP solution are highlighted. For the multiple patches approach, for instance, there are local geometric imperfections at the connection between patches that are not properly handled by the original formulation described in [7]. It assumes smoothness and convexity, which are not guaranteed at such regions. The main novelty of the research is the adaptation of the contact degeneration technique presented in [12] to overcome such local issues.

The next step of the research is to make the LCP formulation more efficient. Since each LCP is independent, the idea is to parallelize its solution in such a way that graphic processing units (GPUs) increase efficiency.

ACKNOWLEDGEMENTS

This works was funded by CNPq (Conselho Nacional de Desenvolvimento Científico e Tecnológico) under the research grant 304321/2021-4.

REFERENCES

[1] P.A. Cundall, O.D.L. Strack, A discrete numerical model for granular assemblies, Géotechnique. 29 (1979) 47–65. https://doi.org/10.1680/geot.1979.29.1.47.

[2] S. He, J. Gan, D. Pinson, A. Yu, Z. Zhou, A discrete element method study of monodisperse mixing of ellipsoidal particles in a rotating drum, Ind Eng Chem Res. 59 (2020) 12458−12470. https://doi.org/10.1021/acs.iecr.9b06623.

[3] A.G. Neto, P. Wriggers, Discrete element model for general polyhedra, Comput Part Mech. (2021). https://doi.org/10.1007/s40571-021-00415-z.

[4] H. Li, G.R. McDowell, Discrete element modelling of under sleeper pads using a box test, Granul Matter. 20 (2018) 1–12. https://doi.org/10.1007/s10035-018-0795-0.

[5] S. Osher, R.P. Fedkiw, Level Set Methods: An Overview and Some Recent Results, J Comput Phys. 169 (2001) 463–502. https://doi.org/10.1006/jcph.2000.6636.

[6] S. Liu, F. Chen, W. Ge, P. Ricoux, NURBS-based DEM for non-spherical particles, Particuology. 49 (2020) 65–76. https://doi.org/10.1016/j.partic.2019.04.005.

[7] M.V. Craveiro, A. Gay Neto, P. Wriggers, Contact between rigid convex NURBS particles based on computer graphics concepts, Comput Methods Appl Mech Eng. 386 (2021) 114097. https://doi.org/10.1016/j.cma.2021.114097.

[8] G. Lu, J.R. Third, C.R. Müller, Discrete element models for non-spherical particle systems: from theoretical developments to applications, Chem Eng Sci. 127 (2015) 425–465. https://doi.org/10.1016/j.ces.2014.11.050.

[9] A. Gay Neto, P. Wriggers, Numerical method for solution of pointwise contact between surfaces, Comput Methods Appl Mech Eng. 365 (2020) 112971. https://doi.org/10.1016/j.cma.2020.112971.

[10] S. Wang, S. Ji, A unified level set method for simulating mixed granular flows involving multiple non-spherical DEM models in complex structures, Comput Methods Appl Mech Eng. 393 (2022) 114802. https://doi.org/10.1016/j.cma.2022.114802.

[11] A. Gay Neto, Framework for automatic contact detection in a multibody system, Comput Methods Appl Mech Eng. 403 (2023) 115703. https://doi.org/10.1016/j.cma.2022.115703.

[12] A. Gay Neto, P. Wriggers, Computing pointwise contact between bodies: a class of formulations based on master–master approach, Comput Mech. 64 (2019) 585–609. https://doi.org/10.1007/s00466-019-01680-9.

[13] A. Gay Neto, Generic interface readily accessible for finite elements (Giraffe) – user’s manual, (2020).

[14] R. McNeel, Rhinoceros 3D, (2022). https://www.rhino3d.com/.

[15] L. Piegl, W. Tiller, The NURBS Book, Springer Berlin Heidelberg, Berlin, Heidelberg, 1995. https://doi.org/10.1007/978-3-642-97385-7.

[16] M. Craveiro, A. Gay Neto, P. Wriggers, DEM simulations using convex NURBS particles, submitted to Comput Part Mech (2023).

[17] C. Ericson, Real-time collision detection, Morgan Kaufmann Publishers, 2005.

[18] J. Nocedal, S.J. Wright, Numerical optimization, Springer New York, 2006. https://doi.org/10.1007/978-0-387-40065-5.

[19] A. Gay Neto, P. Wriggers, Master-master frictional contact and applications for beam-shell interaction, Comput Mech. 66 (2020) 1213–1235. https://doi.org/10.1007/s00466-020-01890-6.

[20] A. Gay Neto, Dynamics of offshore risers using a geometrically-exact beam model with hydrodynamic loads and contact with the seabed, Eng Struct. 125 (2016) 438–454. https://doi.org/10.1016/j.engstruct.2016.07.005.